PHOTONICS Research

Monolithic integration of MoS_2-based visible detectors and GaN-based UV detectors

You Wu,[1,2] Zhiwen Li,[1,2] Kah-Wee Ang,[3] Yuping Jia,[1,2] Zhiming Shi,[1,2] Zhi Huang,[4] Wenjie Yu,[5] Xiaojuan Sun,[1,2] Xinke Liu,[1,2,6] and Dabing Li[1,2,7]

[1]State Key Laboratory of Luminescence and Applications, Changchun Institute of Optics, Fine Mechanics and Physics, Chinese Academy of Sciences, Changchun 130033, China
[2]Center of Materials Science and Optoelectronics Engineering, University of Chinese Academy of Sciences, Beijing 100049, China
[3]Department of Electrical and Computer Engineering, National University of Singapore, Singapore 117583, Singapore
[4]Shenzhen Castle Security Technology Co., Ltd., Shenzhen 518000, China
[5]State Key Laboratory of Functional Materials for Informatics, Shanghai Institute of Microsystem and Information Technology, Chinese Academy of Sciences, Shanghai 200050, China
[6]e-mail: liuxinke@ciomp.ac.cn
[7]e-mail: lidb@ciomp.ac.cn

Received 24 July 2019; revised 30 July 2019; accepted 31 July 2019; posted 1 August 2019 (Doc. ID 373539); published 10 September 2019

With the increasing demand for high integration and multi-color photodetection for both military and civilian applications, the research of multi-wavelength detectors has become a new research hotspot. However, current research has been mainly in visible dual- or multi-wavelength detectors, while integration of both visible light and ultraviolet (UV) dual-wavelength detectors has rarely been studied. In this work, large-scale and high-quality monolayer MoS_2 was grown by the chemical vapor deposition method on transparent free-standing GaN substrate. Monolithic integration of MoS_2-based visible detectors and GaN-based UV detectors was demonstrated using common semiconductor fabrication technologies such as photolithography, argon plasma etching, and metal deposition. High performance of a 280 nm and 405 nm dual-wavelength photodetector was realized. The responsivity of the UV detector reached 172.12 A/W, while that of the visible detector reached 17.5 A/W. Meanwhile, both photodetectors achieved high photocurrent gain, high external quantum efficiency, high normalized detection rate, and low noise equivalent power. Our study extends the future application of dual-wavelength detectors for image sensing and optical communication.

https://doi.org/10.1364/PRJ.7.001127

1. INTRODUCTION

Two-dimensional (2D) layered materials have received extensive attention due to their unique optical and electronic properties [1–10]. Molybdenum disulfide (MoS_2), a typical member of the 2D transition-metal dichalcogenide materials family, has been the most investigated because of its potential applications in high-performance next-generation electrical and optoelectronic devices such as wearable flexible devices, image sensors, and communication devices [11–14]. Compared to the earliest studied graphene (zero bandgap), MoS_2 has a stable band gap associated with the number of material layers varying from 1.2 to 1.8 eV; moreover, the monolayer MoS_2 is a direct band gap (E_g = 1.8 eV) [15]. The MoS_2-based photodetectors (PDs) have achieved significant progress due to their high carrier mobility (~500 $cm^2 \cdot V^{-1} \cdot s^{-1}$), high thermal stability (~1100°C), and high absorbance of MoS_2. Various methods for 2D MoS_2 material preparation have been investigated such as mechanical exfoliation [16], electrochemical exfoliation [17,18], thermal decomposition [19], magnetron sputtering [20], and chemical vapor deposition (CVD) [21–23]. In 2012, an exfoliated single-layer MoS_2 phototransistor was obtained for the first time, and the photoresponsivity was ~7.5 mA/W at 750 nm [16]. Ultrasensitive exfoliated monolayer MoS_2 photodetectors were also demonstrated, showing a distinct photoresponse in the range of 400–680 nm, and the peak photoresponsivity was 880 A/W at a wavelength of 561 nm [24]. The 2D MoS_2 obtained by mechanical exfoliation has a better material quality, but it is uncontrollable and small in size (micrometer scale). Electrochemical exfoliation is also a method of obtaining 2D MoS_2 from top to bottom that can be used to produce larger-scale 2D MoS_2, but with poor quality and problems like interfacial defects also occur when transferring to a target substrate. The CVD growth method has been the most widely investigated because of its excellent repeatability and large size.

SiO_2/Si substrates were used for MoS_2 CVD growth initially because they are perfectly compatible with Si-based optoelectronics [25,26]. However, it was found that it is easier to obtain high-quality MoS_2 on crystalline substrates like sapphire

and GaN [27,28]. These crystal substrates having excellent thermal and chemical stability can be utilized for the preparation of transparent devices. GaN is significantly superior to SiO_2/Si and sapphire substrates because of its nearly perfect lattice matching [29,30] (0.8%, $a_{MoS_2} = 0.316$ nm [31], $a_{GaN} = 0.319$ nm [32]) and the small discrepancy on the thermal expansion coefficients between MoS_2 ($\alpha_{MoS_2} = 4.92 \times 10^{-6}$ K^{-1}) [31] and GaN ($\alpha_{GaN} = 3.95 \times 10^{-6}$ K^{-1} [32]). The almost perfect lattice matching and small difference in thermal expansion coefficient make it possible to grow a higher quality single-layer (SL) MoS_2 on GaN. In addition, it has been demonstrated that the quasiparticle interaction will happen between the 2D MoS_2 and GaN substrate, resulting in the modulation of the intrinsic valley carriers in SL MoS_2, or strong electron-phonon coupling between MoS_2 and GaN can lead to an increasing absorption coefficient of the MoS_2 layer [30]. Figure 1 shows the calculated absorption coefficient of SL MoS_2 in the visible region, in which the value of SL MoS_2/GaN is significantly increased. As a typical representative of the third generation semiconductor, GaN-based materials own the advantages of a wide and direct band gap, good thermal stability, and chemical stability [33], making it one of the best choices for UV photodetector fabrication. High-quality 2D MoS_2 grown on a lattice-matched GaN substrate has the potential to realize new concept high-performance photodetectors with the typical 2D/3D hybrid structure.

With the increasing demand for miniaturization, high integration, and multi-function photodetection, the investigation of 2D/3D multi-wavelength detectors has become a new focus. A hybrid 2D MoS_2/3D GaN heterostructure for dual-functional (405 nm and 532 nm) detection was realized with photoresponsivity on the order of $\sim 10^2$ A/W [34]. Similarly, multilayer MoS_2 grown on a free-standing GaN substrate also showed a multiple-wavelength photoresponse corresponding to 405, 532, and 638 nm, respectively [28]. Two-dimensional MoS_2-based dual-wavelength or multi-wavelength photodetectors have promising applications in future optical communication and image sensors. However, previous research has mainly focused on visible light detection, and this work achieved dual-wavelength detection of the MoS_2-based visible range and the GaN-based UV range. Monolithic integration of UV and visible dual-wavelength detection in this work could broaden optical communications by reducing the signal error rate.

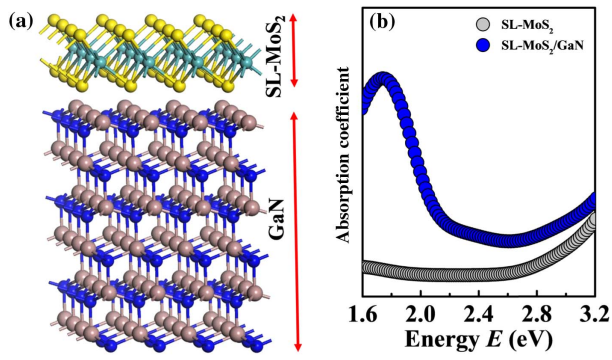

Fig. 1. (a) Illustration of the SL MoS_2-on-GaN structure. (b) Due to the electron-phonon coupling between MoS_2 and GaN, the calculated absorption coefficient of the SL MoS_2 layer is increased significantly in the visible region.

In this work, large-scale SL MoS_2 was grown on a lattice-matched and transparent free-standing (FS) GaN wafer by the CVD method. Common but efficient semiconductor fabrication processes were utilized to obtain monolithic integration of MoS_2-based visible and GaN-based UV detectors. Both the materials and devices were fully characterized. Raman spectroscopy, transmission electron microscopy (TEM), and absorption spectroscopy were used to characterize the as-grown MoS_2 material, proving that a high-quality SL MoS_2 material was obtained. The photoresponsive properties of MoS_2-based visible and GaN-based UV detectors under different incident light power conditions have been investigated. The photoresponsivity R, photoconductive gain G, external quantum efficiency (EQE), noise equivalent power (NEP), normalized detectivity D^*, and the switching characteristics of the monolithic integration dual-wavelength detector were systematically studied in this work.

2. METHOD

A. Sample Preparation and Device Fabrication

A (0001)-oriented Ga face FS-GaN substrate with thickness of ~350 μm was grown by the hydride vapor phase epitaxy (HVPE) method. Ammonia (NH_3) and metal Ga/HCl were used as the nitrogen source and gallium source, respectively, and N_2/H_2 mixed gas was used as the carrier gas. After HVPE growth, it was further polished by chemical mechanical polishing (CMP) to obtain a surface with a surface roughness of 0.2 nm. A two-inch FS-GaN substrate was cut into pieces (1 cm by 1 cm) for the growth process, which is limited by the CVD chamber. The GaN substrate was ultrasonically cleaned with acetone, isopropanol, and deionized water for 10 min each time before being placed in the CVD chamber. 20 mg of molybdenum oxide (MoO_3) was located in an alumina crucible with an FS-GaN substrate upside down on the center of the crucible. 8 g of sulfur (S) powder was laid upstream, and the alumina crucible was located near the center in 100 sccm of argon (Ar) gas flow. The tube was thoroughly cleaned by Ar gas flow to remove air before the growth process. The SL MoS_2 was grown at 750°C for 10 min. The growth temperature has a significant effect on the thickness and shape of the MoS_2 layer. The optimized growth conditions were selected in this study. After the SL MoS_2 was grown on the GaN sample, a photolithography process was performed, and then part of the MoS_2 was etched by the Ar plasma without the protection of the photoresist. Standard photolithography and electron beam evaporation (EBE) for Au electrode (50 nm) preparation were used to define the electrode.

B. Materials and Device Characterizations

The incident laser wavelength of the Raman spectra was 514 nm from an Ar ion laser with laser power of 0.025 mW to avoid laser-induced heat. The absorbance spectra were tested by a UV-visible spectrometer (Shimadzu-2450) from 350 to 800 nm. Current-voltage (I-V) characteristics of the devices were measured by a Keithley 4200-SCS semiconductor analyzer. All measurements of materials and devices were carried out at room temperature.

Corrected: 1 October 2019

3. RESULTS AND DISCUSSION

Figure 2(a) schematically illustrates the MoS_2 growth process by CVD. S powder and MoO_3 were used as precursors, while a Ga-face FS-GaN substrate (1 cm × 1 cm) was placed upside down on the center of the alumina crucible. The MoS_2 growth was completed in an Ar atmosphere with a growth temperature of 750°C for 10 min. The detailed growth process was described in the previous work [35]. The MoS_2 grown on GaN was characterized, and the Raman spectrum was shown in Fig. 2(b). Raman spectrum measurement is based on the Raman scattering effect of the laser passing through the sample, reflecting the interlaminar vibration and intralayer vibration of the material, which is an important means for structural characterization of 2D layered materials [36]. For the Raman spectrum of 2D MoS_2, only E^1_{2g} and A_{1g} optical modes can be observed, which represent the in-plane vibration modes of S and Mo atoms and the out-of-plane vibration modes of S atoms. In addition, the full width at half-maximum (FWHM) of the E^1_{2g} peak characterizes the crystalline quality of 2D MoS_2. The value of FWHM for peak E^1_{2g} here is about 4.6 cm^{-1}, which indicates the high quality of MoS_2. Although the FWHM here is slightly larger than that of mechanical exfoliated MoS_2, large-scale continuous MoS_2 on GaN was obtained by the CVD method in this work. The frequency difference (Δk) between the E^1_{2g} and A_{1g} Raman peaks is also important information for analyzing the thickness of MoS_2. The positions of the E^1_{2g} and A_{1g} peaks are at 384.5 and 403.5 cm^{-1}, respectively, and the frequency difference Δk is about 19 cm^{-1}, corresponding to monolayer MoS_2 which is consistent with other literatures [29,37,38]. An additional strong peak centered at around 418 cm^{-1} was observed, which is in accord with the high-order harmonic frequency of an acoustic phonon of GaN, and is not a Raman active mode [39,40]. Figure 2(c) is the cross-sectional transmission electron microscopy (TEM) image of the MoS_2 grown on GaN substrate. The measured MoS_2 film thickness is ~0.7 nm, indicating a single layer of MoS_2, which is consistent with the Raman measurement result. Figure 2(d) shows the absorbance of the SL-MoS_2 grown on GaN as a function of incident wavelength. There are several absorption peaks in the visible region for SL MoS_2: 430.9, 611.8, and 658.12 nm, respectively, and the absorption at 430.9 nm is the strongest, which is the exciton peak associated with the band edge. The excitonic absorption peaks between 600 and 700 nm observed for MoS_2 arise from the K point of the Brillouin zone [41,42]. The spin-orbit splitting of the valence band of MoS_2 results in an energy difference between the two exciton peaks. Absorbance is the quantification of the absorption intensity, which is defined as $A = \log_{10}(I_0/I_t)$, where I_0 is the intensity of original light and I_t is the intensity of transmitted light [43]. According to the Beer–Lambert law, the relationship between I_t and I_0 is described as $I_t = I_0 e^{-\alpha t}$, where t is the thickness of material and α is the absorption coefficient. The absorption coefficient α is calculated using the formula: $\alpha = \ln(10^A)/t$. A is 0.15 at 405 nm, indicating 29.2% of incident light intensity is absorbed. The thickness of SL MoS_2 is about 0.617 nm. The value of absorption coefficient α calculated in this work is 5.6×10^6 cm^{-1}, which is similar to the absorption coefficient of the multilayer MoS_2 we studied before [28]. The obtained absorption coefficient α of the MoS_2 grown on FS-GaN is about one order of magnitude higher than that of the 2D MoS_2 grown on SiO_2/Si substrate, which may result in a highly responsive MoS_2 photodetector. The high absorption coefficient α in this work could be due to growth on a nearly lattice-matched and a small thermal expansion mismatch FS-GaN substrate, resulting in a high quality of MoS_2.

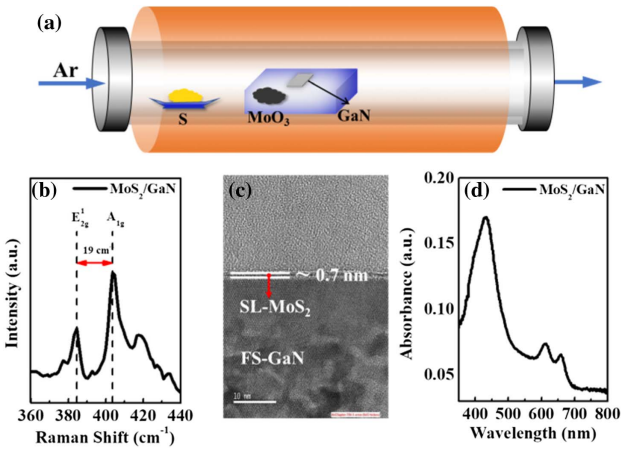

Fig. 2. (a) Illustration of SL MoS_2 growth process by CVD under Ar atmosphere. The FS-GaN substrate was placed upside down on the center of the crucible, and the SL-MoS_2 was grown on the Ga-face. The growth condition was 750°C lasting for 10 min. (b) Raman spectrum of SL-MoS_2 on FS-GaN. (c) Cross-sectional transmission electron microscopy (TEM) image of the MoS_2 grown on the GaN substrate. The measured MoS_2 film thickness is ~0.7 nm, indicating a single layer of MoS_2. (d) Absorbance of SL MoS_2 on the FS-GaN substrate as a function of incident wavelength. The strongest absorption is at around 430 nm.

The schematic diagram of the experimental process for monolithic integration of GaN-based UV detectors and MoS_2-based visible detectors is shown in Fig. 3(a). A large-scale SL MoS_2 was grown on the pre-cleaned FS-GaN substrate by CVD. Then the SL MoS_2 on the FS-GaN sample was etched by Ar plasma to remove part of the MoS_2 that was not protected by photoresist. After the photoresist was removed, an interdigitated Au electrode (50 nm) was prepared on the entire sample to obtain the monolithic integrated GaN PDs and MoS_2 PDs by standard photolithography and metal evaporation. Figure 3(b) is the optical microscope image of monolithic integration of MoS_2-based and GaN-based detectors, and the reference scale in the image is 100 μm. Each photodetector owns an active area of 47,376 μm^2. Figure 3(c) is the 3D schematic view of MoS_2/GaN monolithic integration device. The top view photo image of the fabricated detector is shown in the inset. In this work, monolithic integration of GaN-based detectors and MoS_2-based detectors was achieved in a feasible and low-cost way.

Figure 4(a) shows dark current and light current under 280 nm incident light with different incident power of GaN PDs as a function of voltage, while Fig. 4(b) shows that of MoS_2 PDs under 405 nm laser illumination. Our study before has compared the three different laser wavelengths, 405, 532, and 638 nm. It was found that the MoS_2 PD under the

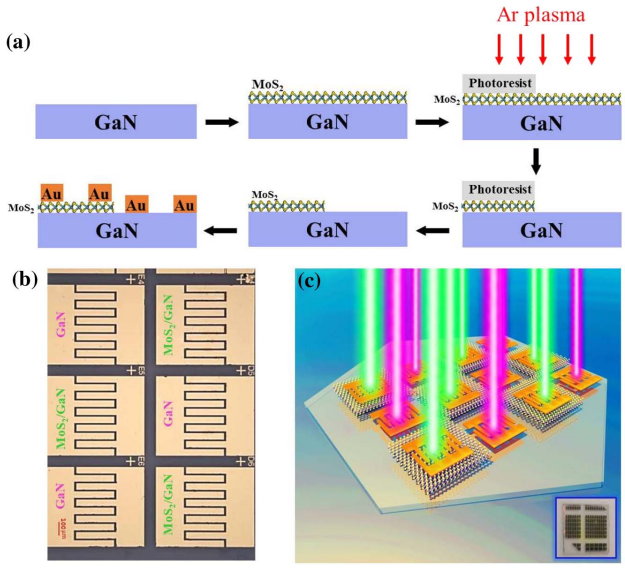

Fig. 3. (a) Schematic diagram of the preparation steps of monolithic integration of GaN-based UV detectors and MoS_2-based visible detectors. Photoresist was used for mask, and part of the SL MoS_2 was etched by Ar plasma. Standard photolithography was applied, and a 50 nm Au electrode was fabricated by electron beam evaporation for the whole wafer. (b) Optical microscope image of monolithic integration of GaN-based and MoS_2-based detectors. The reference scale in the image is 100 μm. (c) 3D schematic view of the MoS_2/GaN monolithic integration device. Top view photo image of 1 cm × 1 cm size sample fabricated is shown in the inset.

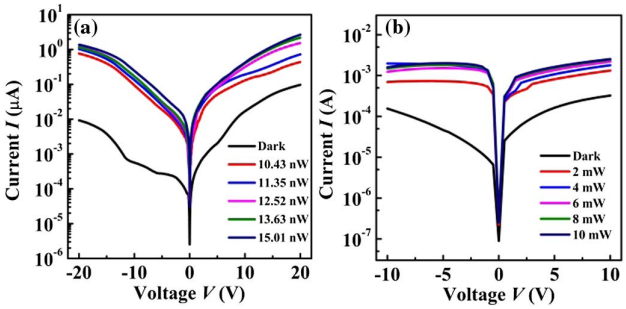

Fig. 4. (a) Dark current and light current for 280 nm incident light under different powers of the GaN PD. (b) Dark current and light current for a 405 nm laser under different incident powers of the MoS_2 PD.

incident light of 405 nm has the best photodetector performance, which is because of a high-photocurrent gain mechanism and high absorption ratio [28]. For 280 nm UV light, it can be absorbed by GaN and then generate photo-generated carriers to achieve UV detection. Thereby, dual-color detection was achieved in this study. The ratio of I_{light}/I_{dark} for GaN PDs is about 10^1–10^2 at a bias voltage of 20 V. It shows as good response to UV light, which is comparable to the results of previous studies [44,45]. As for MoS_2 PDs, the ratio of I_{light}/I_{dark} here is $\sim 10^0$–10^1 at a bias voltage of 3 V.

The photoelectric characteristics of both the GaN-based UV detector and MoS_2 visible detector are calculated as shown in

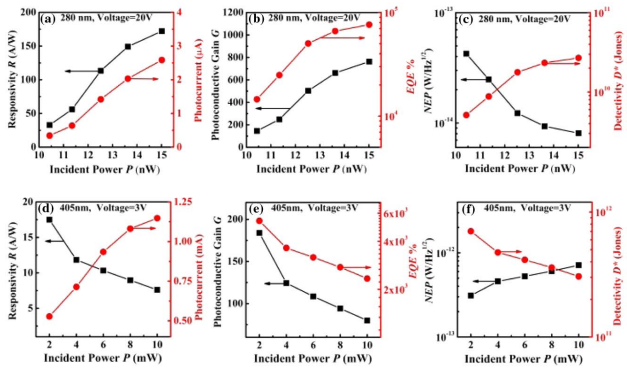

Fig. 5. (a) Responsivity R (A/W) and photocurrent (μA), (b) photoconductive gain G and external quantum efficiency (EQE), and (c) noise equivalent power (NEP) and normalized detectivity D^* of the GaN PD as functions of incident power under a fixed voltage of 20 V. (d) Responsivity R (A/W) and photocurrent (mA), (e) photoconductive gain G and external quantum efficiency (EQE), and (f) noise equivalent power (NEP) and normalized detectivity D^* of the MoS_2 PD as functions of incident power under a fixed voltage of 3 V.

Fig. 5. The responsivity (R), the quantification of the photosensitivity of PDs under certain wavelength light, is described as $R = \frac{I_{ph}}{PA}$, where photocurrent I_{ph} is calculated by $I_{ph} = I_{light} - I_{dark}$, A is the active area of PD, and P is the power density of incident light. Figures 5(a) and 5(d) are photocurrent and responsivity of the GaN PD and MoS_2 PD at 20 V and 3 V, respectively. The peak photoresponsivity of the GaN PD is 172.12 A/W under incident light power of 15 nW, while that of MoS_2 PD is 17.5 A/W under 2 mW laser illumination. This rather high photoresponsivity may be associated with longer carrier lifetime and less carrier recombination in the 2D material under weaker illumination. As shown in Fig. 5(d), as the incident laser power decreases, the R of MoS_2 PD increases slightly, which is in accord with previous reports in MoS_2 and other 2D-based devices [46,47]. When the light power density increased enough, the trap states would be saturated, resulting in the photoresponsivity decrease [48].

Photoconductive gain (G) and EQE of the GaN-based PDs and MoS_2-based PDs were also calculated as shown in Fig. 5(b) and Fig. 5(e), respectively. Photoconductive gain indicates the number of photocurrent carriers generated by absorbing each photon, which can be calculated by the formula $G = \frac{I_{ph}/e}{\mu P/h\nu}$, where e is the elementary charge, ν is the frequency of the incident light, h is the Planck constant, and μ is the absorption percentage. I_{ph} has been calculated in Figs. 5(a) and 5(d). In theory, GaN can absorb light with energy higher than its band gap, so for 280 nm light, $\mu = 1$. The absorption percentage μ of SL MoS_2 at 405 nm is 29.2%, which has been discussed before. The trend of photoconductive gain under different incident power is consistent with that of responsivity. For a GaN UV detector, the maximum photoconductive gain G_{max} of 763.71 was obtained at a voltage of 20 V and an incident light power of 15 nW. The MoS_2 visible detector achieved a G_{max} of 183.88 at 3 V and an incident light power of 2 mW. EQE is the percentage of collected electrons to the total number of incident photons, which can be described as $EQE = \frac{I_{ph}/e}{P/h\nu} = R\frac{h\nu}{q}$.

The maximum EQE of GaN UV detectors reached 76,370.1%, and for MoS_2 visible detectors the maximum EQE is 5369%. Both the GaN-based UV detector and MoS_2-based visible detector exhibit high photoelectric conversion efficiency.

To further evaluate the detectivity and detection limit of our devices, normalized detectivity (D^*) and noise equivalent power (NEP) were calculated as shown in Figs. 5(c) and 5(f) for the GaN UV PD and the MoS_2 visible PD. NEP can evaluate the signal-to-noise ratio more quantitatively, which is defined as the incident optical power at unit signal-to-noise ratio, described as $\mathrm{NEP} = \frac{PA}{S/N}$, where S is signal power and N is noise power [49]. In this work, we can assume that the signal current is the illumination current and the noise current is the dark current (I_d). Therefore, NEP can be calculated by the formula $\mathrm{NEP} = (2eI_d\Delta f)^{\frac{1}{2}}/R$ [49], in which e is the elementary charge amount and Δf is the amplifier bandwidth. A small NEP means that the noise is small, indicating the better performance of the device. The normalized detectivity (D^*), indicating the detection limit to detect the minimum optical signal, is calculated by the equation $D^* = A^{1/2}/\mathrm{NEP}$. The larger D^* means the stronger detection capability of the detector. For a GaN UV detector under 280 nm illumination, NEP is 8.09×10^{-15} – 4.25×10^{-14} W/Hz$^{1/2}$, and D^* is 5.12×10^9 – 2.69×10^{10} Jones. For a MoS_2 visible detector, NEP is 3.10×10^{-13} – 7.14×10^{-13} W/Hz$^{1/2}$, and D^* is 7.02×10^{11} – 3.05×10^{11} Jones. The performance of the MoS_2-based PD in this work is much lower than that of Si-based PDs (R of ~300 A/W and D^* of ~10^{13} Jones) [50,51], but it is better than the SL MoS_2-based PD (R of 7.5 mA/W) [16]. This work achieved monolithic integration of GaN-based UV PD and MoS_2-based visible PD for the first time to our knowledge in a simple process; however, the performance of the detectors is still not ideal, and further optimization of CVD growth details and device fabrication optimization are necessary.

Photo-switching characteristics have also been investigated for both GaN-based and MoS_2-based PDs at a fixed voltage under 280 nm and 405 nm wavelength of incident light illumination, respectively. Figures 6(a) and 6(c) show the photocurrent of the GaN PD and MoS_2 PD under periodic changes in dark and illumination conditions. When under-illuminated, the current rises to the on state and then falls to the off state under the dark condition. The switch ratio of devices is described as $\frac{\mathrm{ON}}{\mathrm{OFF}} = \frac{I_{\mathrm{light}}}{I_{\mathrm{dark}}}$. For GaN-based UV PD, the ratio of photocurrent versus dark is about 27.4, while that of MoS_2-based visible PD is about 13.5. The switching behavior is quite stable through multiple times of changing the illumination conditions. The rise time (t_{rise}) of the photodetectors is usually defined as the time it takes for the current to increase from 10% to 90% of the maximum, and the fall time (t_{fall}) is the time for current decreasing from 90% to 10%. For a GaN UV detector, t_{rise} is 0.21 s and t_{fall} is 0.22 s as shown in Fig. 6(b); for MoS_2 visible detector, t_{rise} is 1.36 s and t_{fall} is 8.31 s as shown in Fig. 6(d). t_{rise} and t_{fall} obtained in this work are shorter than that of graphene-based devices [52], but are comparable to the reported SL MoS_2-based PDs [24]. For MoS_2-based PD, when the laser turns off, the photocurrent decays to the dark level exponentially. It is observed that the sustained photocurrent is because of the long-range Coulomb potential captured, which may be related to the charged impurities in the interface of MoS_2/GaN or inside MoS_2, therefore greatly affecting the recombination of electron-hole pairs. The proper device passivation or packaging technology can further improve the photocurrent switching performance of the device, which is also the next step for us to improve the performance.

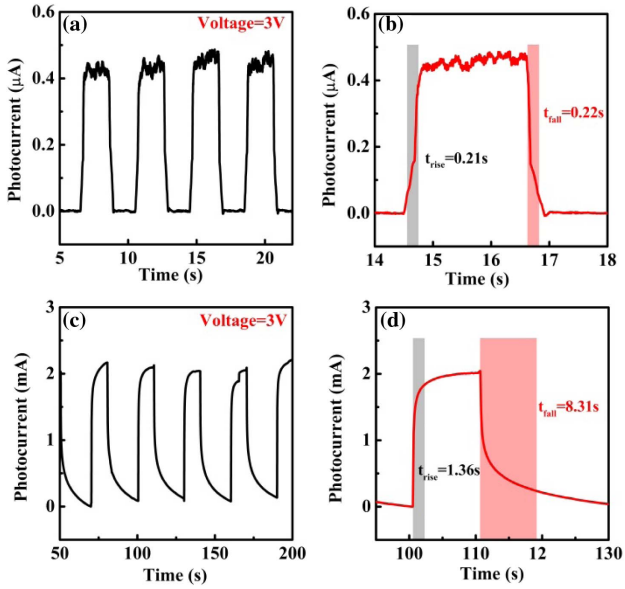

Fig. 6. Photocurrent as a function of time under alternative dark and illumination. (a) Photocurrent-time curve of GaN illuminated by a 280 nm light source with the incident power of 15.01 nW at 20 V. (b) The rise time (from 10% to 90% of maximum photocurrent) and the fall time (from 90% to 10% of maximum photocurrent) of the GaN PD. (c) Photocurrent-time curve of MoS_2/GaN illuminated by a 405 nm laser with the incident power of 10 mW at 3 V. (d) The rise and fall time of the MoS_2/GaN PD.

4. CONCLUSION

In this work, the CVD growth method was used to obtain a high-quality and large-scale monolayer MoS_2 on a nearly lattice matched free-standing GaN substrate. And by a low-cost and feasible process, monolithic integration of MoS_2-based visible detectors and GaN-based UV detectors was realized. The responsivity of the UV detector reached 172.12 A/W under 280 nm illumination, while that of the visible detector reached 17.5 A/W under 405 nm laser. Meanwhile, high-photocurrent gain G, high external quantum efficiency, high normalized detectivity, and low noise equivalent power have been achieved for both two kinds of photodetectors. This study provides a low-cost, easy-to-process method for the preparation of dual-wavelength detectors with monolithic integrated UV and visible light, which has promising applications in image sensing and optical communication devices.

Funding. National Key Research and Development Plan (2017YFB0403000); National Science Fund for Distinguished Young Scholars (61725403); National Natural Science Foundation of China (61874118, 61704171, 61504083, 61674161); CAS Pioneer Hundred Talents Program; Jilin

Provincial Science & Technology Department (20180201026 GX); Key Program of the International Partnership Program of CAS (181722KYSB20160015); Special Project for Inter-government Collaboration of the State Key Research and Development Program (2016YFE0118400); Youth Innovation Promotion Association of CAS; Guangdong Province Key Research and Development Plan (2019B010138002).

Acknowledgment. We thank Prof. Ke Xu from Suzhou Institute of Nano-Tech and Nano-Bionics, Chinese Academy of Sciences, for useful discussion and Prof. Hao-Chung Kuo from Taiwan Chiao Tung University. You Wu and Zhiwen Li contributed equally to this work.

REFERENCES

1. R. Cao, H. Wang, Z. Guo, D. K. Sang, L. Zhang, Q. Xiao, Y. Zhang, D. Fan, J. Li, and H. Zhang, "Black phosphorous/indium selenide photoconductive detector for visible and near-infrared light with high sensitivity," Adv. Opt. Mater. **7**, 1900020 (2019).
2. M. Zhao, Z. Ye, R. Suzuki, Y. Ye, H. Zhu, J. Xiao, Y. Wang, Y. Iwasa, and X. Zhang, "Atomically phase-matched second-harmonic generation in a 2D crystal," Light Sci. Appl. **5**, e16131 (2016).
3. A. K. Geim and I. V. Grigorieva, "Van der Waals heterostructures," Nature **499**, 419–425 (2013).
4. Z. Guo, S. Chen, Z. Wang, Z. Yang, F. Liu, Y. Xu, J. Wang, Y. Yi, H. Zhang, L. Liao, P. K. Chu, and X.-F. Yu, "Metal-ion-modified black phosphorus with enhanced stability and transistor performance," Adv. Mater. **29**, 1703811 (2017).
5. K. S. Novoselov, A. Mishchenko, A. Carvalho, and A. H. C. Neto, "2D materials and van der Waals heterostructures," Science **353**, aac9439 (2016).
6. Y. Abate, S. Gamage, Z. Li, V. Babicheva, M. H. Javani, H. Wang, S. B. Cronin, and M. I. Stockman, "Nanoscopy reveals surface-metallic black phosphorus," Light Sci. Appl. **5**, e16162 (2016).
7. M. Zhang, Q. Wu, F. Zhang, L. Chen, X. Jin, Y. Hu, Z. Zheng, and H. Zhang, "2D black phosphorus saturable absorbers for ultrafast photonics," Adv. Opt. Mater. **7**, 1800224 (2019).
8. J. Yang, R. Xu, J. Pei, Y. W. Myint, F. Wang, Z. Wang, S. Zhang, Z. Yu, and Y. Lu, "Optical tuning of exciton and trion emissions in monolayer phosphorene," Light Sci. Appl. **4**, e312 (2015).
9. Q. Ou, Y. Zhang, Z. Wang, J. A. Yuwono, R. Wang, Z. Dai, W. Li, C. Zheng, Z.-Q. Xu, X. Qi, S. Duhm, N. V. Medhekar, H. Zhang, and Q. Bao, "Strong depletion in hybrid perovskite p-n junctions induced by local electronic doping," Adv. Mater. **30**, 1705792 (2018).
10. Y. Zhang, C.-K. Lim, Z. Dai, G. Yu, J. W. Haus, H. Zhang, and P. N. Prasad, "Photonics and optoelectronics using nano-structured hybrid perovskite media and their optical cavities," Phys. Rep. **795**, 1–51 (2019).
11. J. Wang, I. Verzhbitskiy, and G. Eda, "Electroluminescent devices based on 2D semiconducting transition metal dichalcogenides," Adv. Mater. **30**, 1802687 (2018).
12. K. F. Mak and J. Shan, "Photonics and optoelectronics of 2D semiconductor transition metal dichalcogenides," Nat. Photonics **10**, 216–226 (2016).
13. J. Y. Lee, J.-H. Shin, G.-H. Lee, and C.-H. Lee, "Two-dimensional semiconductor optoelectronics based on van der Waals heterostructures," Nanomaterials **6**, 193 (2016).
14. M. Buscema, J. O. Island, D. J. Groenendijk, S. I. Blanter, G. A. Steele, H. S. J. van der Zant, and A. Castellanos-Gomez, "Photocurrent generation with two-dimensional van der Waals semiconductors," Chem. Soc. Rev. **44**, 3691–3718 (2015).
15. S. Manzeli, D. Ovchinnikov, D. Pasquier, O. V. Yazyev, and A. Kis, "2D transition metal dichalcogenides," Nat. Rev. Mater. **2**, 17033 (2017).
16. Z. Yin, H. Li, H. Li, L. Jiang, Y. Shi, Y. Sun, G. Lu, Q. Zhang, X. Chen, and H. Zhang, "Single-layer MoS_2 phototransistors," ACS Nano **6**, 74–80 (2012).
17. N. Liu, P. Kim, J. H. Kim, J. H. Ye, S. Kim, and C. J. Lee, "Large-area atomically thin MoS_2 nanosheets prepared using electrochemical exfoliation," ACS Nano **8**, 6902–6910 (2014).
18. Y. Yang, H. Hou, G. Zou, W. Shi, H. Shuai, J. Li, and X. Ji, "Electrochemical exfoliation of graphene-like two-dimensional nanomaterials," Nanoscale **11**, 16–33 (2019).
19. R. Zhuo, Y. Wang, D. Wu, Z. Lou, Z. Shi, T. Xu, J. Xu, Y. Tian, and X. Li, "High-performance self-powered deep ultraviolet photodetector based on MoS_2/GaN p-n heterojunction," J. Mater. Chem. C **6**, 299–303 (2018).
20. N. Goel, R. Kumar, B. Roul, M. Kumar, and S. B. Krupanidhi, "Wafer-scale synthesis of a uniform film of few-layer MoS_2 on GaN for 2D heterojunction ultraviolet photodetector," J. Phys. D **51**, 374003 (2018).
21. W. Zhang, J.-K. Huang, C.-H. Chen, Y.-H. Chang, Y.-J. Cheng, and L.-J. Li, "High-gain phototransistors based on a CVD MoS_2 monolayer," Adv. Mater. **25**, 3456–3461 (2013).
22. X. Ling, Y. Lee, Y. Lin, W. Fang, L. Yu, M. S. Dresselhaus, and J. Kong, "Role of the seeding promoter in MoS_2 growth by chemical vapor deposition," Nano Lett. **14**, 464–472 (2014).
23. H. Shan, Y. Yu, X. Wang, Y. Luo, S. Zu, B. Du, T. Han, B. Li, Y. Li, J. Wu, F. Lin, K. Shi, B. Tay, Z. Liu, X. Zhu, and Z. Fang, "Direct observation of ultrafast plasmonic hot electron transfer in the strong coupling regime," Light Sci. Appl. **8**, 9 (2019).
24. O. Lopez-Sanchez, D. Lembke, M. Kayci, A. Radenovic, and A. Kis, "Ultrasensitive photodetectors based on monolayer MoS_2," Nat. Nanotechnol. **8**, 497–501 (2013).
25. N. Perea-López, Z. Lin, N. R. Pradhan, A. Iñiguez-Rábago, A. L. Elías, A. McCreary, J. Lou, P. M. Ajayan, H. Terrones, L. Bali, and M. Terrones, "CVD-grown monolayered MoS_2 as an effective photosensor operating at low-voltage," 2D Mater. **1**, 011004 (2014).
26. Z. Cheng, M. Xia, S. Liu, R. Hu, G. Liang, and S. Zhang, "Role of rough substrate on the growth of large single-crystal MoS_2 by chemical vapor deposition," Appl. Surf. Sci. **476**, 1008–1015 (2019).
27. D. Dumcenco, D. Ovchinnikov, K. Marinov, P. Lazi, M. Gibertini, N. Marzari, O. L. Sanchez, Y.-C. Kung, D. Krasnozhon, M.-W. Chen, S. Bertolazzi, P. Gillet, A. F. I. Morral, A. Radenovic, and A. Kis, "Large-area epitaxial monolayer MoS_2," ACS Nano **9**, 4611–4620 (2015).
28. X. Liu, Y. Chen, D. Li, S.-W. Wang, C.-C. Ting, L. Chen, K.-W. Ang, C.-W. Qiu, Y.-L. Chuen, X. Sun, and H.-C. Kuo, "Nearly lattice-matched molybdenum disulfide/gallium nitride heterostructure enabling high-performance phototransistors," Photon. Res. **7**, 311–317 (2019).
29. P. Yan, J. Wang, G. Yang, N. Lu, G. Chu, X. Zhang, and X. Shen, "Chemical vapor deposition of monolayer MoS_2 on sapphire, Si and GaN substrates," Superlattices Microstruct. **120**, 235–240 (2018).
30. Y. Wan, J. Xiao, J. Li, X. Fang, K. Zhang, L. Fu, P. Li, Z. Song, H. Zhang, Y. Wang, M. Zhao, J. Lu, N. Tang, G. Ran, X. Zhang, Y. Ye, and L. Dai, "Epitaxial single-layer MoS_2 on GaN with enhanced valley helicity," Adv. Mater. **30**, 1703888 (2018).
31. R. Murray and B. L. Evans, "The thermal expansion of 2H-MoS_2 and 2H-WSe_2 between 10 and 320 K," J. Appl. Crystallogr. **12**, 312–315 (1979).
32. K. Wang and R. R. Reeber, "Thermal expansion of GaN and AlN," Mat. Res. Soc. Symp. Proc. **12**, 863–868 (1998).
33. D. Li, K. Jiang, X. Sun, and C. Guo, "AlGaN photonics: recent advances in materials and ultraviolet devices," Adv. Opt. Photon. **10**, 43–110 (2018).
34. C.-Y. Huang, C. Chang, G.-Z. Lu, W.-C. Huang, C.-S. Huang, M.-L. Chen, T.-N. Lin, J.-L. Shen, and T.-Y. Lin, "Hybrid 2D/3D MoS_2/GaN heterostructures for dual functional photoresponse," Appl. Phys. Lett. **112**, 233106 (2018).
35. X. Liu, J. He, Q. Liu, D. Tang, J. Wen, W. Liu, W. Yu, J. Wu, Z. He, Y. Lu, D. Zhu, W. Liu, P. Cao, S. Han, and K.-W. Ang, "Low temperature carrier transport study of monolayer MoS_2 field effect transistors prepared by chemical vapor deposition under an atmospheric pressure," J. Appl. Phys. **118**, 124506 (2015).
36. K.-G. Zhou, F. Withers, Y. Cao, S. Hu, G. Yu, and C. Casiraghi, "Raman modes of MoS_2 used as fingerprint of vander Waals interactions in 2-D crystal-based heterostructures," ACS Nano **8**, 9914–9924 (2014).

37. C. Lee, H. G. Yan, L. E. Brus, T. F. Heinz, J. Hone, and S. Ryu, "Anomalous lattice vibrations of single-and few-layer MoS_2," ACS Nano **4**, 2695–2700 (2010).
38. P. Yan, Q. Tian, G. Yang, Y. Weng, Y. Zhang, J. Wang, F. Xie, and N. Lu, "Epitaxial growth and interfacial property of monolayer MoS_2 on gallium nitride," RSC Adv. **8**, 33193–33197 (2018).
39. H. Siegle, G. Kaczmarczyk, L. Filippidis, A. P. Litvinchuk, A. Hoffmann, and C. Thomsen, "Zone-boundary phonons in hexagonal and cubic GaN," Phys. Rev. B **55**, 7000–7004 (1997).
40. V. Y. Davydov, Y. E. Kitaev, I. N. Goncharuk, and A. N. Smirnov, "Phonon dispersion and Raman scattering in hexagonal GaN and AlN," Phys. Rev. B **58**, 12899 (1998).
41. K. F. Mak, C. Lee, J. Hone, J. Shan, and T. F. Heinz, "Atomically thin MoS_2: a new direct-gap semiconductor," Phys. Rev. Lett. **105**, 136805 (2010).
42. A. Splendiani, L. Sun, Y. Zhang, T. Li, J. Kim, C.-Y. Chim, G. L. Galli, and F. Wang, "Emerging photoluminescence in monolayer MoS_2," Nano Lett. **10**, 1271–1275 (2010).
43. W. Choi, M. Y. Cho, A. Konar, J. H. Lee, G. Cha, S. C. Hong, S. Kim, J. Kim, D. Jena, J. Joo, and S. Kim, "High-detectivity multilayer MoS_2 phototransistors with spectral response from ultraviolet to infrared," Adv. Mater. **24**, 5832–5836 (2012).
44. L. Liu, C. Yang, A. Patanè, Z. Yu, F. Yan, K. Wang, H. Lu, J. Li, and L. Zhao, "High-detectivity ultraviolet photodetectors based on laterally mesoporous GaN," Nanoscale **9**, 8142–8148 (2017).
45. D. Li, X. Sun, H. Song, Z. Li, Y. Chen, H. Jiang, and G. Miao, "Realization of a high-performance GaN UV detector by nanoplasmonic enhancement," Adv. Mater. **24**, 845–849 (2012).
46. S. Li, X. Chen, F. Liu, Y. Chen, B. Liu, W. Deng, B. An, F. Chu, G. Zhang, S. Li, X. Li, and Y. Zhang, "Enhanced performance of a CVD MoS_2 photodetector by chemical *in situ* n-type doping," ACS Appl. Mater. Interfaces **11**, 11636–11644 (2019).
47. F. Gong, F. Wu, M. Long, F. Chen, M. Su, Z. Yang, and J. Shi, "Black phosphorus infrared photodetectors with fast response and high photoresponsivity," Phys. Status Solidi (RRL) **12**, 1800310 (2018).
48. J.-Y. Wu, Y. T. Chun, S. Li, T. Zhang, J. Wang, P. K. Shrestha, and D. Chu, "Broadband MoS_2 field-effect phototransistors: ultrasensitive visible-light photoresponse and negative infrared photoresponse," Adv. Mater. **30**, 1705880 (2018).
49. P. Hu, L. Wang, M. Yoon, J. Zhang, W. Feng, X. Wang, Z. Wen, J. C. Idrobo, Y. Miyamoto, D. B. Geohegan, and K. Xiao, "Highly responsive ultrathin GaS nanosheet photodetectors on rigid and flexible substrates," Nano Lett. **13**, 1649–1654 (2013).
50. Y. Guo, G. Yu, and Y. Liu, "Functional organic field-effect transistors," Adv. Mater. **22**, 4427–4447 (2010).
51. X. Gong, M. Tong, Y. Xia, W. Cai, J. S. Moon, Y. Cao, G. Yu, C.-L. Shieh, B. Nilsson, and A. J. Heeger, "High-detectivity polymer photodetectors with spectral response from 300 nm to 1450 nm," Science **325**, 1665–1667 (2009).
52. F. Xia, T. Mueller, Y.-M. Lin, A. Valdes-Garcia, and P. Avouris, "Ultrafast graphene photodetector," Nat. Nanotechnol. **4**, 839–843 (2009).

Corrected: 1 October 2019